Filter Bank-Driven Multivariate Synchronization Index for Training-Free SSVEP BCI

Ke Qin, Raofen Wang, and Yu Zhang

***Abstract*— In recent years, multivariate synchronization index (MSI) algorithm, as a novel frequency detection method, has attracted increasing attentions in the study of brain-computer interfaces (BCIs) based on steady state visual evoked potential (SSVEP). However, MSI algorithm is hard to fully exploit SSVEP-related harmonic components in the electroencephalogram (EEG), which limits the application of MSI algorithm in BCI systems. In this paper, we propose a novel filter bank-driven MSI algorithm (FBMSI) to overcome the limitation and further improve the accuracy of SSVEP recognition. We evaluate the efficacy of the FBMSI method by developing a 6-command SSVEP-NAO robot system with extensive experimental analyses. An offline experimental study is first performed with EEG collected from nine subjects to investigate the effects of varying parameters on the model performance. Offline results show that the proposed method has achieved a stable improvement effect. We further conduct an online experiment with six subjects to assess the efficacy of the developed FBMSI algorithm in a real-time BCI application. The online experimental results show that the FBMSI algorithm yields a promising average accuracy of 83.56% using a data length of even only one second, which was 12.26% higher than the standard MSI algorithm. These extensive experimental results confirmed the effectiveness of the FBMSI algorithm in SSVEP recognition and demonstrated its potential application in the development of improved BCI systems.**

***Index Terms*— Brain-computer interface, EEG signal, filter bank, multivariate synchronization index, NAO robot, steady-state visual evoked potential.**

I. Introduction

BRAIN-COMPUTER Interface (BCI) is a new interactive technology for the human brain to realize direct control over external hardware devices [1], [2]. By decoding the brain signals from electrical activities in the cerebral cortex, human's intention can be identified and converted into the control instructions of external devices. That is, a BCI system does not rely on external muscle and peripheral nerve pathways. Also, it can provide humans with additional interactive channels [3], [4]. In recent years, an increasing number of research efforts have been dedicated to the development of BCI systems [5], [6], with applications extended from the realization of wheelchair operation [7], prosthetic control [8], neurological rehabilitation [9] for physically challenged patients to a wider range of practical scenarios, such as virtual reality games [10], military detection [11] and operator fatigue detection [12], [13]. Depending on the specific activity patterns of the brain, EEG signals applied to BCI development mainly include: slow cortical potential (SCP) [14], P300 evoked potential [15], [16], steady-state visual evoked potential (SSVEP) [17], [18], event-related desynchronization (ERD) and synchronization (ERS) [19], [20]. Among them, SSVEP has recently attracted extensive attention from BCI researchers due to its high signal-to-noise ratio and outstanding information transfer rate [21]–[23].

Over the past decades, significant progress has been made in the development of SSVEP-based BCIs [2], [5]. It was mainly driven by efforts from the two aspects: i) the induced paradigm and ii) the recognition algorithm. By incorporating phase information into the induction paradigm [24], the stimulus frequency achievable with the computer monitor is no longer limited by the fixed refresh rate of the screen, which greatly increases the achievable control categories of the SSVEP-based BCI system. In terms of recognition algorithm, after the canonical correlation analysis (CCA) method [25] commonly replaced the traditional power spectral density analysis [26] (PSDA), the multi-channel SSVEP signal recognition algorithms were gradually developed [27]–[30]. Zhang *et al.* [27] proposed a multiway canonical correlation analysis (MCCA). By maximizing the correlation between the multidimensional signal and the two-dimensional reference signal to get the optimized reference signal. Pan *et al.* [28] used the occipital single-channel EEG signal SSVEP response stage to estimate the phase, proposed a phase constrained CCA (p-CCA) algorithm and successfully applied it to SSVEP-BCI. Zhang *et al.* [29] applied L1 regularization to trial path array optimization in MCCA, and proposed a more powerful L1-MCCA algorithm than MCCA. Zhang *et al.* [30] extracted the common features of SSVEP from multiple sets of EEG data recorded at the same stimulation frequency, optimized the reference signal completely based on the training data, and proposed a method based on multiset CCA (Mset-CCA). These methods have shown superior performance to the standard CCA algorithm in many respects, but the standard

Manuscript received January 11, 2021; revised March 11, 2021; accepted April 5, 2021. Date of publication April 14, 2021; date of current version May 25, 2021. This work was supported in part by the Natural Science Foundation of China under Grant 61803255 and in part by the Natural Science Foundation of Shanghai under Grant 18ZR1416700. *(Corresponding author: Raofen Wang.)*

Ke Qin and Raofen Wang are with the College of Electronic and Electrical Engineering, Shanghai University of Engineering Science, Shanghai 201600, China (e-mail: qkpaper@163.com; rfwangsues@163.com).

Yu Zhang is with the Department of Bioengineering, Lehigh University, Bethlehem, PA 18015 USA (e-mail: yuzi20@lehigh.edu).

Digital Object Identifier 10.1109/TNSRE.2021.3073165

CCA method is still used by many authors for baseline testing of SSVEP systems and is active in the field of BCI [31]–[33].

In recent years, the Multivariate synchronization index (MSI) [34] algorithm has been validated as a feature extraction method that is superior to CCA. Zhang *et al.* [35] further improved the frequency recognition accuracy of SSVEP by using the time-local information of SSVEP signal when modeling the covariance matrix according to previous studies [36], [37]. An extension of MSI algorithm [38] was also developed based on the literature [39], [40] which combined the delayed version of the EEG data to improve the effectiveness of the CSP algorithm, resulting in higher recognition accuracy and an information transfer rate (ITR). However, current frequency identification systems based on the standard MSI algorithm or its variants cannot take the full advantage of harmonic components in SSVEP signal. To address this problem, filter bank strategy has been introduced into BCI systems [41], [42], which aims to get more robustly decode EEG patterns by exploiting multi-band information [43]. Ang *et al.* [41] have applied the filter bank common space pattern (FBCSP) method to EEG power feature extraction in the μ and β bands, significantly improving the recognition accuracy of different motion image states. Chen *et al.* [42] applied filter banks analysis to the improvement of CCA algorithm, proposed a filter bank CCA (FBCCA) algorithm and successfully applied it in SSVEP-BCI. Accordingly, we consider that the filter bank approach has the potential to significantly improve the performance of the SSVEP-BCI based MSI algorithm.

In this study, we propose filter bank-driven MSI (FBMSI) algorithm to improve SSVEP frequency recognition. Our study designs a 6-command SSVEP BCI system with 10-15Hz (1Hz interval) as the stimulus frequencies, and verifies the FBMSI algorithm with the system for NAO robot control. Firstly, this study uses offline SSVEP experimental signals to discuss the requirements of the filtering range and the harmonic number of reference signal in FBMSI algorithm. In order to optimize the subband design in the filter bank, a four-subband division method is proposed ((F1): each subband contains one harmonic frequency band; (F2) each subband contains three harmonic frequency bands; (F3) each subband contains five harmonic frequency bands; (F4) the upper cut-off frequency of each subband is 105 Hz). In addition, this paper also explores two subband weight assignment formulas E1 and E2, and compares the different enhancement effects of the two weight formulas on the SSVEP system. Finally, subband decomposition is performed using method F4, and online BCI experiments are performed in six subjects using the weight formula E1. The experimental results showed that the method significantly improved the individual identification performance of the SSVEP frequencies and improved the overall identification accuracy and information transfer rate (ITR).

The following sections are arranged as follows: Section 2 introduced signal acquisition and data preprocessing, Section 3 introduced the FBMSI algorithm flow proposed in this paper, Section 4 discussed and analyzed the results of FBMSI algorithm, and Section 5 discussed and summarized the results.

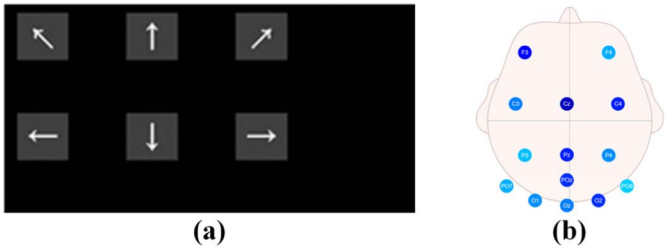

Fig. 1. Experimental stimulation interface and experimental lead.

II. Signal Acquisition and Experiment Setup

A. Experiment Setup

In this study, a six-command SSVEP stimulation interface was designed to provide control instructions to the robot, as shown in Fig 1(a). The stimulation frequency was 10-15 Hz (with an interval of 1 Hz) and the arrows represent the motion control command of the robot. During the experiments, EEG signals were recorded by a 16-channel wireless physiological signal acquisition system produced by NEURACLE. The sampling frequency was 1000 Hz and the 16 channels were placed using the international 10-20 system standard, as shown in Fig 1(b). The electrode impedance of each channel was kept below 15kΩ. The 6-command SSVEP stimulation matrices (each with a size of 3×3 cm) were displayed on a 23.5-inch Samsung LCD (C24F396FHC) screen with a refresh frequency of 60 Hz. The stimulation software was developed in MATLAB's Psychological Toolbox (PTB). Prior to the experiment, each subject is informed about the content and procedure of the experiment and signs an informed consent form.

B. Offline Experiment

Nine healthy subjects (six males and three females, aged 22-26 years, mean age: 24 years) with normal or corrected normal vision participated in the data collection of the offline experiment. The offline experiment consisted of 30 blocks, each containing 12 trials. At the beginning of each trial, a red square marker would appear at the target stimulus location. Subjects were required to turn their attention to the marker within 1 second. The target frequency box flashed for 3 seconds, with a minute break between each block. The offline experiment was designed to provide sufficient training data for the FBMSI algorithm, so it was not necessary to drive the NAO robot during this procedure. A total of 360 trials per subject were performed in the offline experiments.

C. Online Experiment

The online BCI experimental design is illustrated in Fig 2. The visual stimulus evoked the subjects' SSVEP signal, and the EEG cap (signal acquisition device) sent the collected EEG signal to the signal synchronizer through Bluetooth. The online BCI experiment adopted synchronization control, so it was necessary to strictly synchronize the start time of SSVEP stimulation with the collected EEG signals. The error of the signal synchronizer used in this paper had an error of less than 1ms. The synchronized EEG signals were sent to the FBMSI

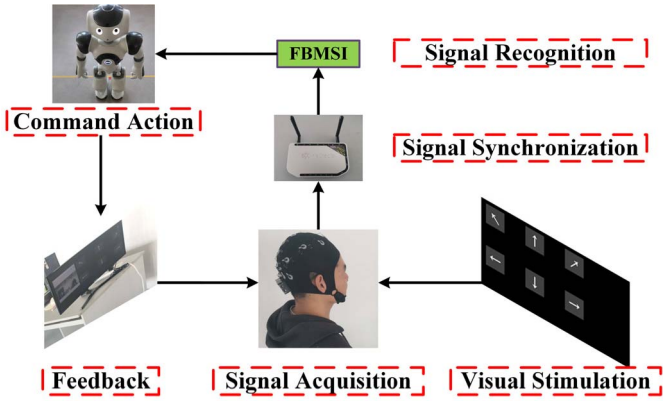

Fig. 2. Flow chart of online experiment.

algorithm recognition module through TCP/IP protocol, and the target instruction was identified by the effective SSVEP segment in EEG signals. Then, the target instruction could be sent to the NAO robot to drive the action. The camera of the NAO robot's head can give visual feedback to the subject. The NAO robot's stride length was set to 20 cm, and the execution time for each action was approximately 3s. The online BCI experiment consisted of 6 blocks, each containing 12 trials and each trial lasted for 5s (1s of visual stimuli, 1s of target cues, and 3s of NAO robot movement time). After target recognition, the subjects were provided with visual feedback from the NAO robot's camera and the next target prompt was initiated. The online data analysis program was implemented in the MatlabR2020a environment.

D. Data Preprocessing

The collected raw EEG signals were downsampled to 250Hz. The nine channels (Pz, P3, P4, POz, PO7, PO8, Oz, O1, and O2) in parietal and occipital regions were used for the experimental analysis, as they contained the most informative SSVEP components [33]. In vision systems, a delay process of vision should be considered [42], [44]. As suggested in literature [42], a 140-ms time delay was chosen for the SSVEP analysis in our study. As a result, the extraction ranges of offline and online experimental data were [0.14, 3.14]s and [0.14, 1.14]s, respectively. Finally, the offline experimental data sample for the EEG sample used for data analysis is 9 (number of channels) × 750 (sampling points) × 360 (trials) × 9 (number of subjects); the online experimental data sample for the EEG sample used for performance validation is 9 (number of channels) × 300 (sampling points) × 72 (trials) × 6 (number of subjects).

III. Method

A. The Standard MSI Algorithm

The key step of the standard MSI algorithm is to calculate the synchronization index between two multivariate signals for frequency identification. Let $\mathbf{X} \in \mathbf{R}^{N1\times M}$ and $\mathbf{Y} \in \mathbf{R}^{N2\times M}$ (N_1 and N_2 are the channels of the two signals, M is the signal sampling length) respectively represent multivariate EEG signals and reference signal. Among them, reference signal $\mathbf{Y}$ is constructed as follows:

$$Y_f = \begin{bmatrix} \sin(2\pi ft) \\ \cos(2\pi ft) \\ \cdots \\ \sin(2\pi N_h ft) \\ \cos(2\pi N_h ft) \end{bmatrix}, \quad t = \frac{1}{f_s}, \frac{2}{f_s}, \frac{3}{f_s}, \ldots, \frac{M}{f_s} \tag{1}$$

where f_s is the sampling frequency, N_h represents the number of harmonics used in the calculation process and f is the target stimulation frequency. Without loss of generality, both signals need to be standardized to have a zero mean and unit variance. The calculation process is as follows:

Firstly, the joint correlation matrix between $\mathbf{X}$ and $\mathbf{Y}$ should be calculated as:

$$C = \begin{bmatrix} C_{11} = \frac{1}{M} XX^T & C_{12} = \frac{1}{M} XY^T \\ C_{21} = \frac{1}{M} YX^T & C_{22} = \frac{1}{M} YY^T \end{bmatrix} \tag{2}$$

Cross-correlation matrix (C12, C21) and autocorrelation matrix (C11, C22) make up the joint correlation matrix. But the existence of the autocorrelation matrix will affect the synchronization computing. Therefore, the following linear transformation is employed to remove the influence of auto-correlation matrix in the joint correlation matrix:

$$U = \begin{bmatrix} C_{11}^{-\frac{1}{2}} & 0 \\ 0 & C_{22}^{-\frac{1}{2}} \end{bmatrix} \tag{3}$$

Then, the new joint correlation matrix can be described as follows:

$$R = UCU^T = \begin{pmatrix} \mathrm{I}_1 & C_{11}^{-\frac{1}{2}} C_{12} C_{22}^{-\frac{1}{2}} \\ C_{22}^{-\frac{1}{2}} C_{21} C_{11}^{-\frac{1}{2}} & \mathrm{I}_2 \end{pmatrix} \tag{4}$$

The autocorrelation matrix on the main diagonal is eliminated by introducing the unit matrices $\mathbf{I}_1 \in \mathbf{R}^{N1\times N1}$ and $\mathbf{I_2} \in \mathbf{R}^{N2\times N2}$. Then, the new joint correlation matrix $\mathbf{R}$ is decomposed into eigenvalues to obtain eigenvalues λ_1, λ_2, …, $\lambda_{P(P=N1+N2)}$, which can be calculated to obtain the normalized eigenvalues λ'_i:

$$\lambda'_i = \lambda_i / \sum_{i=1}^{P} \lambda_i = \lambda_i / tr(R) \tag{5}$$

Finally, the formula for calculating the synchronization index of $\mathbf{X}$and $\mathbf{Y}$is as follows:

$$S = 1 + \sum_{i=1}^{P} \lambda'_i \log(\lambda'_i) / \log(P) \tag{6}$$

From (2), if $\mathbf{X}$and $\mathbf{Y}$ are completely uncorrelated, $C_{12} = C_{21} = 0$, then $\mathbf{C}$ transformed by $\mathbf{U}$ is a diagonal matrix, thus $S_{\min} = 0$, $\lambda_i = 1$. Instead, if $\mathbf{X}$and $\mathbf{Y}$ are perfectly synchronous, the matrix $\mathbf{R}$ will consist of four unit matrixes. It is not difficult to conclude that half of the matrix eigenvalues are 2 and the rest are 0. According to (6), when the number of $\mathbf{X}$ and $\mathbf{Y}$ channels is only one, S gets the maximum value, $S_{max} = 1$. For other conditions, $S_{max} = log(2)/log(P)$.

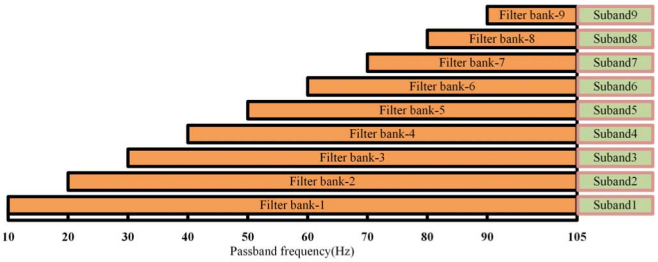

Fig. 3. Frequency range corresponding to each subband of the FBMSI algorithm, with the frequency range of the Nth subband being [10*N 105] Hz.

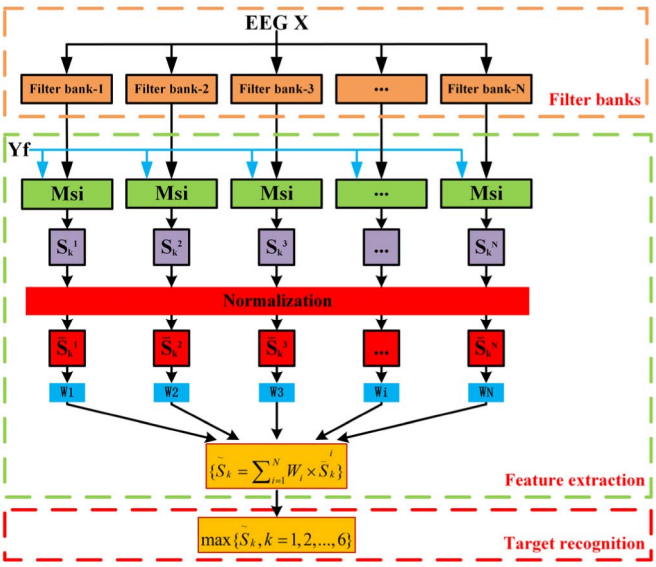

Fig. 4. Flow chart of FBMSI algorithm.

Based on (6), the identification of SSVEP can be realized. With (7), K indices, S_1, $S_2, \ldots, S_K$ are obtained with K reference signals. Then, the target frequency f_{target} could be recognized.

$$f_{t\arg et} = \max_k S_k \quad k = 1, 2, \ldots, K \tag{7}$$

B. FBMSI Algorithm

In order to take full advantage of the harmonic components of SSVEP signals, the FBMSI algorithm was proposed by combining MSI and filter bank strategy. With reference to the filter bank design method in [42], a total of 9 fourth-order Chebyshev zero-phase filters were designed to decompose the SSVEP signal into 9 subbands ($X_{Filterbank-N}$, N represents the subband index, $N = 1, \ldots\ldots, 9$). By extracting the harmonic components from each subband, a better recognition effect than the standard MSI method could be achieved. The method of subband division was shown in Fig 3. In this study, the stimulation frequency was 10-15 Hz, and the lower cutoff frequency of each subband was 10^* N Hz. 105Hz was chosen as the upper cutoff frequency of each subband (the best results were obtained at this cutoff frequency).

Fig 4 illustrated the framework flow of the proposed algorithm. After the decomposition of the filter bank, the synchronization indices of the subband signal and the sine-cosine reference signal were calculated separately. For the kth target stimulus frequency, the synchronization index vector S was composed of the synchronization index calculation for the N sub-band signals.

$$S = \begin{bmatrix} S_k^1 \\ S_k^2 \\ \cdots \\ S_k^N \end{bmatrix} = \begin{bmatrix} MSI(X_{Filterbank-1}, Y_f) \\ MSI(X_{Filterbank-2}, Y_f) \\ \cdots \\ MSI(X_{Filterbank-N}, Y_f) \end{bmatrix} \tag{8}$$

The MSI ($X_{Filterbank-N}$, Y_f) represented the synchronization index $S_k N$ between the Nth subband signal and the reference signal, which was normalized to between [0,1] and multiplied by the weight vector W. Among them, the normalization layer in the FBMSI algorithm is to improve the optimization effect of parameters a and b as much as possible. If the difference between the calculated values for the different subbands is too large, the high-frequency subbands are characteristically submerged in the low-frequency subbands because the calculated values are too small, which limits the optimization ability of parameters a and b. Therefore, we designed a normalization layer to map the computational results of the filter between 0 and 1. Since the SNR of the SSVEP harmonic components decreases as the response frequency increases, the weight coefficient W_N for each subband component is defined by the following power exponential formula E1:

$$E1 : W_N = N^{-a} + b, \quad N \in [19] \tag{9}$$

where N represents the index of the subband, a and b represents the constant parameters to be optimized. In order to reduce the computational time and effort, and to facilitate the visual expression of the parameters at the same time, the final optimization range of parameter a is [0, 2]. Parameter b represents the baseline weight of each sub-band and is developed to compensate for the lack of a power exponent N^{-a} that reduces subband weight too rapidly. According to (9), each sub-band has an equal baseline weight, the range of parameter b is designed to be [0, 1].

In this study, the classification performance of the FBMSI algorithm was evaluated with parameters a and b optimized using grid method based on offline data. The synchronization exponential vectors of each subband, which had been scaled by the weight vectors, were summed together. The obtained results could be regarded as the feature vectors obtained by feature extraction. Wherein, the maximum synchronization index corresponds to the index K corresponding to the target frequency, thus realizing the target recognition of SSVEP signal.

IV. FBMSI Algorithm Optimization and Results Analysis

As described in Section 3, the FBMSI algorithm performs standard MSI calculations based on the subband decomposition of the original EEG signal. The conditions that affected the recognition accuracy of MSI algorithm include: the number of harmonics in the reference signal and the filter range. In order to improve the recognition accuracy of the FBMSI algorithm, these two conditions need to be optimized. In addition, in the discussion of [42], it was found that not all subbands are beneficial for target recognition. Therefore,

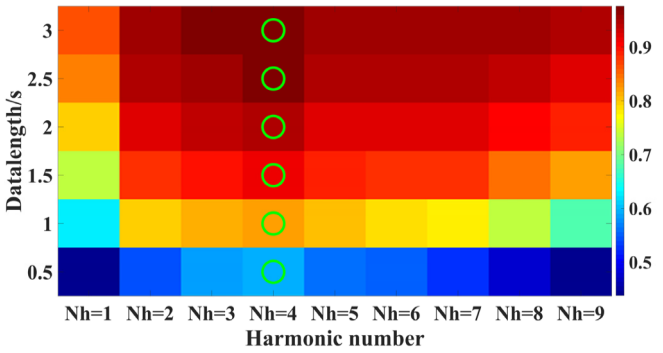

Fig. 5. Relationship between the number of harmonics and recognition accuracy under different signal lengths. The green circles represented the highest recognition accuracy obtained at different signal lengths (3s: 97.59%, 2.5s: 96.98%,2s: 94.57%, 1.5s: 90.99%, 1s: 82.22%, 0.5s: 59.48%).

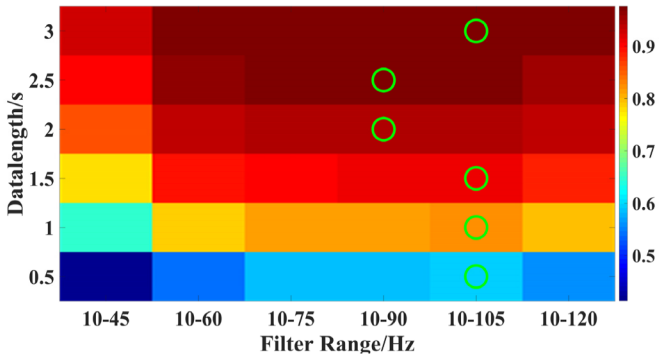

Fig. 6. The relationship between recognition accuracy and filter range under different signal lengths. The green circles represent the highest recognition accuracy at different signal lengths. Under different filtering ranges (left to right), the number of subband decomposition was set as follows: 3, 5, 7, 8, 9, 9.

it was also necessary to optimize the number of subbands decompositions. Thus, this section discussed the number of harmonics, the filter range, and the number of subbands suitable for the FBMSI algorithm firstly. Then, the improvement effect of the FBMSI algorithm was evaluated using offline data under optimal conditions. Finally, online testing was used to verify the robustness of the optimization results and whether the optimization conditions caused overfitting.

A. Optimization of Number of Harmonics for FBMSI Algorithm

In MSI-related algorithms, the number of harmonics in the reference signal is closely related to the recognition accuracy. In [33], [35], satisfactory results were obtained using $Nh = 2$. While in [38], optimal results were obtained using $Nh = 3$. Similarly, the recognition effect of the FBMSI algorithm also depended on the harmonic number Nh of the reference signal. Fig 5 showed the relationship between the number of harmonics and the recognition accuracy at different signal lengths (0.5-3s in steps of 0.5). Colorbar showed the relationship between color and recognition accuracy. It was not difficult to conclude from Fig 5 that the recognition accuracy of FBMSI increased gradually with increasing signal length. At $Nh = 4$, the FBMSI algorithm achieved the highest recognition accuracy at different signal lengths. Therefore, $Nh = 4$ is the most suitable reference signal harmonic number for the FBMSI algorithm.

B. Optimization of Analysis of Harmonics for FBMSI Algorithm

In the frequency domain, for each frequency of the SSVEP stimulation, the subjects' EEG signals produced energy spikes at both the fundamental and octave frequencies of the stimulus frequency. For the application of SSVEP filter range, there were no fixed conclusions [33], [35], [38], [42]. Therefore, the filter range of FBMSI was discussed in this study, and Fig 6 showed the relationship between filter range and recognition accuracy (0.5-3s in steps of 0.5) under different signal lengths. Colorbar showed the relationship between color and recognition accuracy. The demand for filtering range was also slightly different for different signal lengths. The peaks of recognition accuracy were mainly concentrated in the two filter ranges of 10-90 Hz and 10-105 Hz. Among them, 10-90Hz: 97.47%, 97.04%, 94.63%, 90.74%, 81.64%, 58.92%, 10-105 Hz: 97.59%, 96.98%, 94.57% 90.99%, 82.22%, 59.48%. Although the best recognition accuracy was obtained in the filtered range of 10-90Hz for signal lengths at 2s and 2.5s, it did not differ significantly from that of 10-105Hz (97.04% vs 96.98%, 94.63% vs 94.57%). On the contrary, under short-time SSVEP signals (0.5s,1s), the recognition accuracy of 10-105Hz was about 0.5% higher than that of 10-90Hz (82.22% vs. 81.64%, 59.48% vs. 58.92%). Therefore, 10-105Hz was chosen as the filter range for the FBMSI algorithm.

C. Optimization and Analysis of Subband Decomposition Number for FBMSI Algorithm

SSVEP components contained in the EEG signals were observed to vary along with the signal length. In general, SSVEP components of subjects become more stable as the stimulation time increased [17]. Our study suggested that the number of subband decomposition (SDN) required for EEG signals with different SSVEP components was different. In short, the change of signal length may affect the required SDN in the FBMSI algorithm. Therefore, this paper discussed the minimum SDN required to achieve the maximum recognition accuracy at different signal lengths. As can be seen from Fig 7, the demand for SDN from SSVEP signal decreased with the increase of data length. This indicated that there is no need for too many subbands to extract features when the EEG signal contains sufficient SSVEP components. When the stimulus time is short and the SSVEP component of the EEG signal is small, it is necessary to decompose the original EEG signal into more subbands to obtain more features. Therefore, the required SDNs of FBMSI algorithm in SSVEP signal recognition process with different time lengths are also different.

D. The Improved Effect of FBMSI Algorithm

In order to better interpret the improvement principle of the FBMSI algorithm, EEG (target frequency: 15 Hz) signal with a time length of 3s was taken to analyze as an example.

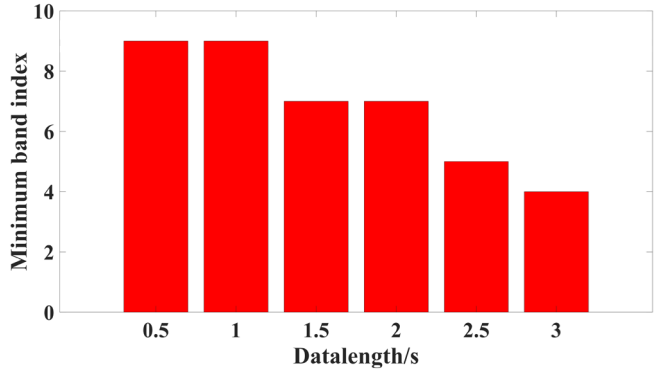

Fig. 7. The minimum SDN required to identify the maximum accuracy for different data lengths (in second). Each SDN represents the largest subband index of the original EEG signal decomposition under the signal length.

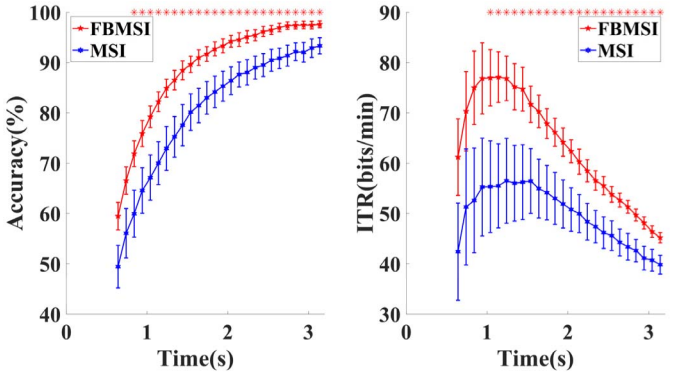

Fig. 9. Average recognition accuracy and ITR of FBMSI algorithm under different signal lengths. Error bars represent standard deviation. Asterisks indicat significant difference between the two methods (*: $p < 0.05$).

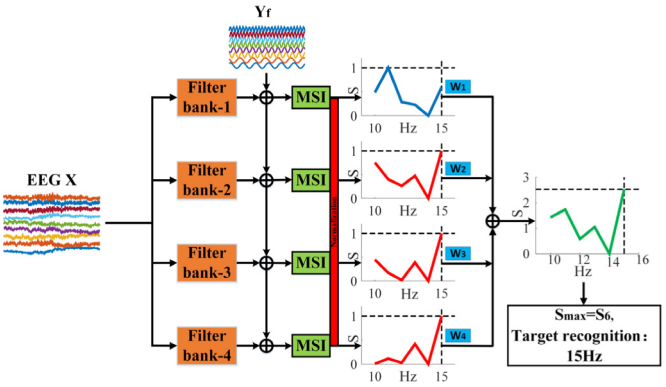

Fig. 8. Illustration of the FBMSI algorithm for the recognition of SSVEP at a target stimulus frequency of 11 Hz. The FBMSI method corrected the MSI identification result (12 Hz) to 15 Hz (FB-1:10-105 Hz, FB-2:20-105 Hz, FB-3:30-105 Hz, FB-4:40-105 Hz).

TABLE I
RECOGNITION ACCURACY AND ITR IN ONLINE SSVEP-NAO ROBOT EXPERIMENT

Subject	Accuracy(%)	ITR(bits/min)
Subject1	75.00	62.80
Subject2	93.06	108.41
Subject3	84.72	84.92
Subject4	76.39	65.70
Subject5	80.56	74.88
Subject6	91.67	104.09
Mean±Std	83.56±7.63	83.47±19.32

According to the discussion in Section 4.3, only four subbands were needed at a time length of 3s. After the original EEG signal passed through four different filters, the synchronization index with sine-cosine reference signal was calculated separately. In Fig 8, the blue line represents the synchronization index of the six stimulus frequencies calculated by the standard MSI algorithm. It can be seen that MSI misidentified the target frequency as 12 Hz. While in the other filter calculations (red line), the maximum value was reached at 15 Hz. After the superposition of the weight vector W, a spike was finally formed at the target frequency of 15 Hz, which improved the recognition effect.

Fig 9 compares the BCI performance of our developed FBMSI model and the standard MSI algorithm in relation to signal length (0.64-3.14s, step size 0.1s). It can be seen that FBMSI achieved better results than standard MSI for both recognition accuracy and ITR across various signal lengths. Moreover, in the range of 1.14-3.14s, FBMSI and standard MSI showed significant differences in recognition accuracy and ITR, and the paired T-test showed that $p < 0.05$. At 1s, FBMSI obtained the highest ITR, 76.18 bits/min. Compared to standard MSI (52.73 bits/min), the improvement was nearly 50%. Therefore, in this study, a data length of 1 s was selected for the online SSVEP experiment. At this time, the average recognition accuracy of FBMSI algorithm was 82.22%, which was 12.22% higher than that of MSI algorithm (70.00%).

Fig 10 shows the parameters of FBMSI when the data length is 1s. For FBMSI algorithm, the larger the SDN required, the more filters would be used, resulting in higher computational cost. If the same parameter combination achieved the same optimal recognition effect under different SDNs, it was obvious that the smallest SDN was the best choice. Fig 10(a) shows the minimum SDN required to achieve maximum recognition accuracy for each combination of parameters a and b. Fig 10(b) shows the recognition effect for all combinations of parameters a and b with SDN = 9. The green circles in Figs 10(a) and 10(b) represent the optimal combination of parameters: SDN = 9, a = 2, and b = 0.1.

E. Performance of FBMSI Algorithm in Online BCI

Table I showed the recognition accuracy and ITR of all subjects in the online SSVEP experiment. Since the movement time of the NAO robot varied for different action commands, only the time for stimulation and calculation were included in the calculation of ITR.

In the online recognition system, the number of reference signal harmonics *Nh* was 4, the high frequency cutoff frequency was 105 Hz, and SDN = 9. In the online experiment, the average recognition accuracy for all subjects was 83.56 ± 7.63% and the average ITR was 83.47 ± 19.32 bits/min. Both evaluation indicators were slightly higher than the results in the training data (acc: 82.22%, ITR: 76.18 bits/min). These slight

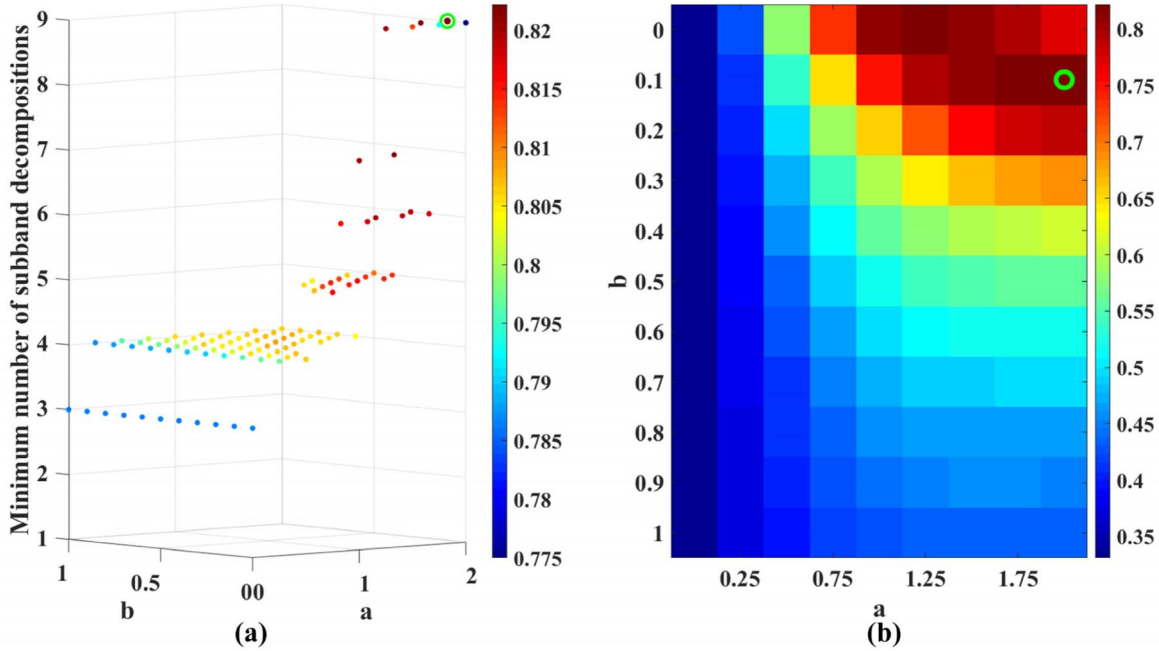

Fig. 10. Recognition accuracy of the weight parameters (a, b) in FBMSI obtained by grid method optimization. (a) The minimum SDN required to achieve the highest recognition accuracy under each combination of parameters a and b. The green circle represented the highest recognition accuracy among all combinations (82.22%). (b) The recognition effect for each weighted parameter combination at SDN = 9. The green circle represents the optimal combination of parameters: SDN = 9, a = 2, b = 0.1.

differences may be caused by the differences between the subjects in the two experiments. The paired T-test showed no significant difference ($P > 0.05$) between the two experimental results of six subjects who participated in both offline and online experiment. In this study, based on the collected online experimental data, MSI algorithm was used to analyze the online data. The results showed that FBMSI had a significantly better recognition accuracy than MSI under different numbers of harmonics ($Nh = 1$:65.05%, $Nh = 2$:71.99%, $Nh = 3$:70.37%, $Nh = 4$:71.30%, $Nh = 5$:72.92%, $Nh = 6$:73.15%, $Nh = 7$:72.69%, $Nh = 8$: 71.86%). The proposed method got 12.26% higher than standard MSI ($Nh = 4$) in recognition accuracy (offline enhancement: 12.22%). It is noteworthy that the overall result comparison could prove that the parameter optimization result of FBMSI did not appear

overfitting phenomenon and exhibited strong robustness. At the same time, these results also demonstrate the effectiveness and feasibility of the FBMSI algorithm in online SSVEP-based BCI.

V. Discussion and Summary

A. Filter Bank Design of FBMSI Algorithm

In the design process of the filter bank, the filter range is the first factor to be determined. In our study, FBMSI achieved the best results at the upper cutoff frequency of 105 Hz, which was slightly different from the upper cutoff frequency of 90 Hz in [42], indicating that optimization of the upper cutoff frequency may be the direction of development to improve the performance of the filter bank algorithm.

In order to explore the design optimization method of the filter bank, three design methods were proposed and compared with the filter banks designed in this paper:

(F1) Each subband contained one harmonic band, as shown in Fig 11(a). Filter range: {10*N, min [15*N, 105]} Hz.

(F2) Each subband contained three harmonic bands, as shown in Fig 11(b). Filter range: {10*N, min [15*3*N, 105]} Hz.

(F3) Each subband contained five harmonic bands, as shown in Fig 11(c). Filter range: {10*N, min [15*5*N, 105]} Hz.

(F4) The upper cutoff frequency of each subband is 105Hz, as shown in Fig 11(d). Filter range: {10*N, min [15*N, 105]} Hz.

Fig 12 shows the SSVEP recognition accuracies obtained by the four methods at different signal lengths. With the increase of harmonic frequency bands contained in each subband, the recognition accuracy increased gradually. The paired T-test showed that the FBMSI algorithm under the four filter bank design methods had significant difference in recognition accuracy from the standard MSI algorithm ($P < 0.05$). However, among the four design methods, there were significant differences between F1 and others ($P < 0.05$). Although F4 achieved the highest recognition accuracy at different data lengths, there were no significant differences among F2, F3, and F4($P > 0.05$). Therefore, the three methods were validated by using the data collected from online experiment. The results showed that the F4 method again achieved the highest recognition accuracy (F2:81.48%, F3:82.87%, F4:83.56%). These results may indicate that the recognition effect would improve as the number of frequency bands contained in each subband increased.

B. Subband Weight Formula of FBMSI Algorithm

The advantage of FBMSI was not only to decompose the SSVEP signal into subbands to make more effective use of the harmonic components, but more importantly in the use

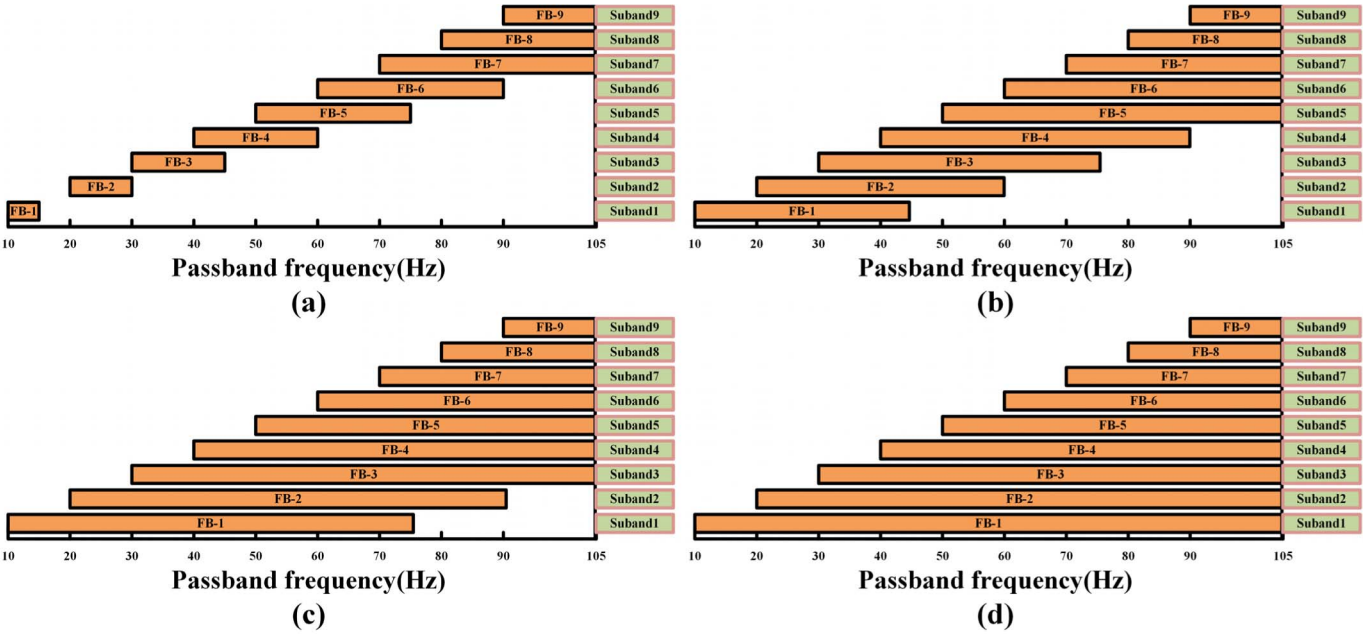

Fig. 11. Subband division corresponding to the four methods of FBMSI algorithm in filter design. (a) F1, (b) F2, (c) F3, (d) F4.

of (9) give the subbands appropriate weight coefficients. The subband weight coefficients obtained by the corresponding optimization and the subbands made FBMSI have a stable improvement effect on MSI. This paper also compared another weighting formula E2:

$$E2 : W_N = a\exp^{-bN} + c, \quad N \in [19] \tag{10}$$

where N denotes the index of the subband, and a, b,c are constants (a, b $\in$ [0, 2], c $\in$ [0, 1]). Compared with (9), the corresponding subband weight coefficients decrease more stable. And the value of each subband weight coefficient was more average. Similarly, this study used grid method to optimize E2 based on offline data to achieve the optimal classification performance, where the step size of a, b was 0.25, and the step size of c was 0.1. The results were shown in Fig 13.

Fig 13(a) shows the recognition accuracy of both methods E1 and E2 at different signal lengths. With the increase of signal length, the difference of recognition accuracy between the two methods gradually decreased. But the results of E1 method were higher than that of E2 method in all cases. Fig 13(b) showed the minimum SDN required to achieve the optimal recognition accuracy at different signal lengths. Interestingly, the method E2 did not show the same pattern of method E1 (Roughly, the longer the signal length is, the smaller SDN is required), but only required four or five filters, i.e., only four or five subbands were needed to decompose the SSVEP signals. Although the recognition accuracy of E2 was slightly lower than that of method E1, the number of required filters was much smaller than method E1 in short-time SSVEP signals (0.6-1.6s). This means that more than half of the computational cost could be saved during the recognition of short-time SSVEP signals. In the hardware configuration of this study, the computational cost increases by about 4ms for each additional filter, and the cost would increase with the decrease of hardware configuration. Therefore, E2 method is more suitable for SSVEP recognition system with lower hardware configuration, which reduces the computational cost and increases the real-time performance of the system at a slight sacrifice of accuracy.

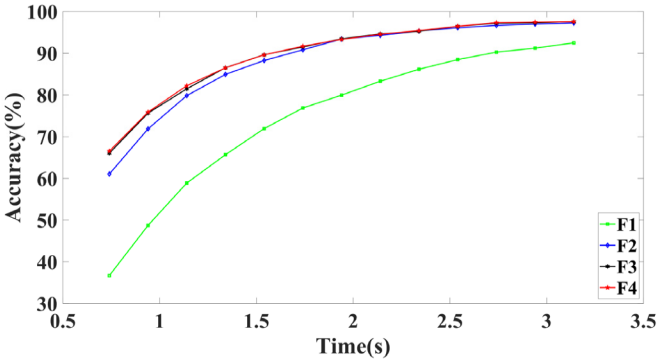

Fig. 12. Under four filter bank design methods, recognition accuracy of FBMSI algorithm at different data lengths (0.74-3.14s, step size 0.2s).

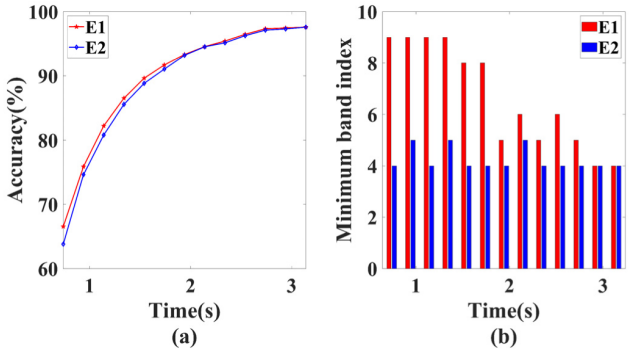

Fig. 13. Different performance of the two weight formulas in FBMSI. (a) The recognition accuracy of E1 and E2 methods at different signal lengths. (b) The minimum number of filters required for E1 and E2 to achieve the highest recognition accuracy at different signal lengths.

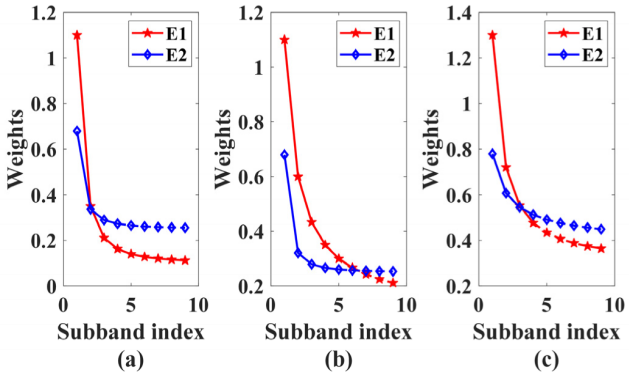

Fig. 14. Weighting coefficients of FBMSI algorithm under E1 and E2. (a): signal length = 1 s, (b): signal length = 2 s, (c): signal length = 3 s. The red and blue dashed lines represent the weight coefficients of the unused subbands of E1 and E2.

C. Weight Variation of FBMSI Algorithm

In order to investigate the relationship between the weight coefficient and the signal length, we further investigated the variation of the weight coefficient of E1, E2 under three signal lengths (1s, 2s, and 3s). The results were shown in Fig 14. For the convenience of presentation, the lower cutoff frequency of each subband shall prevail, and subbands above 50 Hz were referred to as high-frequency subbands (HFS) and vice versa as low-frequency subbands (LHS).

By comparing the weight coefficients under three signal lengths, it was obviously found that the weight coefficients of LHS became higher as the signal length increases. The reason for this phenomenon was similar to that discussed in Section 4.3: when EEG signals contain sufficient SSVEP components, it is unnecessary to extract too many subbands to obtain harmonic information. Instead, the HFS at this time could be considered as noise. When the stimulation time is shorter and the SSVEP component of the EEG signal is unstable, more subbands need to be extracted to obtain harmonic information. At this time, the effective information implied by the HFS will be beneficial to the identification of target frequency. However, this does not mean that increasing the weight of HFS can improve the recognition performance of short-time SSVEP signals. Comparing the two weight formulas, E2 gives a relatively stable weight coefficient for HFS. But the effective subband is limited to LFS, which means that HFS does not enter the recognition process. This phenomenon indicates that giving too high weight to HFS is not beneficial to the target recognition. From these results, E1 gives a lower weight to HFS according to the power exponent., which accordingly achieved better results.

D. Comparison With Other Methods

In recent years, Zhang *et al.* [35], [38] has developed two powerful variants of MSI. In [35], the algorithm called time-localized MSI (TMSI) measured correlation based on the entropy of the normalized eigenvalues of the multichannel signals covariance matrix at hyperparameters $\tau = 24$, v = 3. Paper [38] proposed an extension of MSI (EMSI) method by using a time delay method, where the best identification results were obtained when the hyperparameter $\tau = 1$. This paper also compared the CCA algorithm with its improved algorithm based on the filter bank, FBCCA [42]. Reference [42] decomposed the original EEG signal into 10 subbands to improve the frequency detection of the CCA algorithm. In order to make a more comprehensive comparison of these methods, we also used the Benchmark dataset [45] of Tsinghua University, corresponding to the experimental target frequency, 1224 pieces of data (subject 5 data download failed) were intercepted at [0.64 1.64] (the stimulus started at 0.5s) for analysis. The parameter setting and identification results of each method are shown in Table II.

TABLE II
COMPARISON OF THE PROPOSED FBMSI METHOD WITH OTHER METHODS

Methods	Accuracy(%) Our Online Dataset	Accuracy(%) Benchmark Dataset
MSI $_{(Nh=4)}$	71.30%	68.13%
EMSI $_{(\tau=1,\ Nh=4)}$	77.55%	73.45%
TMSI $_{(\tau=6,\ V=3,\ Nh=3)}$	81.71%	74.59%
CCA $_{(Nh=5)}$	70.60%	64.79%
FBCCA $_{(a=1.25,\ b=0.25,\ Nh=5)}$	82.64%	76.63%
FBMSI $_{(a=2,\ b=0.1,\ Nh=4)}$	**83.56%**	**78.27%**

As can be seen from Table II, the recognition accuracy of the various methods, when tested on Benchmark dataset, is slightly reduced. Regarding the gap in the identification accuracy of the two datasets, there are two reasons for our analysis: (1) In Tsinghua University's dataset, the short target cue time is only 0.5s, compared with 1s in our experiment, and (2) In the case of short prompt times, two-thirds of the subjects in Tsinghua University's dataset were naive subjects, that's not friendly for target recognition.

Although the identification accuracy of various methods decreased slightly, our proposed method still achieved the highest identification effect. Also, the lift effect on the MSI algorithm is above 10%, demonstrating that our improvement on the MSI algorithm has a stable lift effect. Those comparison results showed that the FBMSI algorithm had good recognition performance, which proved the effectiveness and feasibility of the FBMSI algorithm in training -free SSVEP-based BCI.

VI. CONCLUSION

To fully exploit the SSVEP-associated harmonic components in EEG signals, we modified MSI with filter bank strategy and proposed a filter bank driven MSI algorithm (FBMSI) for further improvement of SSVEP recognition in BCI applications. Four subband decomposition methods were designed to compare in the framework of this algorithm, and method F4 was found to have the best recognition effect and stability. Furthermore, our study also compared the effects of two weight formulas, E1 and E2, on the BCI effect. Among them, E1 had the best recognition effect, but E2 could improve the real-time performance of the system with lower hardware configuration at a slight sacrifice of recognition accuracy. The results of both off-line and online experiments showed that the method significantly reduced the recognition error rate of

standard MSI algorithm and greatly improved the recognition accuracy and real-time transmission rate of SSVEP-BCI.

REFERENCES

[1] J. N. Mak and J. R. Wolpaw, "Clinical applications of brain-computer interfaces: Current state and future prospects," *IEEE Rev. Biomed. Eng.*, vol. 2, no. 1, pp. 187–199, Dec. 2009.

[2] J. Wolpaw, N. Birbaumer, D. McFarland, G. Pfurtscheller, and T. Vaughan, "Brain-computer interfaces for communication and control," *Clin. Neurophys.*, vol. 113, no. 6, pp. 767–791, 2002.

[3] M. A. Lebedev and M. A. L. Nicolelis, "Brain-machine interface: Past, present and future," *Trends Neuroe.*, vol. 29, no. 9, pp. 536–546, Sep. 2006.

[4] L. F. Nicolas-Alonso and J. Gomez-Gil, "Brain computer interfaces, a review," *Sensors*, vol. 12, no. 2, pp. 1211–1279, 2012.

[5] P. Konrad and T. Shanks, "Implantable brain computer interface: Challenges to neurotechnology translation," *Neurobiol. Disease*, vol. 38, no. 3, pp. 369–375, Jun. 2010.

[6] J. R. Wolpaw, "Brain-computer interfaces as new brain output pathways," *J. Physiol.*, vol. 579, no. 3, pp. 613–619, Mar. 2007.

[7] Y. Li, J. Pan, F. Wang, and Z. Yu, "A hybrid BCI system combining P300 and SSVEP and its application to wheelchair control," *IEEE Trans. Biomed. Eng.*, vol. 60, no. 11, pp. 3156–3166, Nov. 2013.

[8] P. Horki, T. Solis-Escalante, C. Neuper, and G. Müller-Putz, "Combined motor imagery and SSVEP based BCI control of a 2 DoF artificial upper limb," *Med. Biol. Eng. Comput.*, vol. 49, no. 5, pp. 567–577, May 2011.

[9] A. Frisoli *et al.*, "A new gaze-BCI-Driven control of an upper limb exoskeleton for rehabilitation in real-world tasks," *IEEE Trans. Syst., Man, Cybern. C, Appl. Rev.*, vol. 42, no. 6, pp. 1169–1179, Nov. 2012.

[10] L. Bonnet, F. Lotte, and A. Lecuyer, "Two brains, one game: Design and evaluation of a multiuser BCI video game based on motor imagery," *IEEE Trans. Comput. Intell. AI Games*, vol. 5, no. 2, pp. 185–198, Jun. 2013.

[11] C. Barngrover, A. Althoff, P. DeGuzman, and R. Kastner, "A brain–computer interface (BCI) for the detection of mine-like objects in sidescan sonar imagery," *IEEE J. Ocean. Eng.*, vol. 41, no. 1, pp. 123–138, Jan. 2016.

[12] R. Wang, Y. Zhang, and L. Zhang, "An adaptive neural network approach for operator functional state prediction using psychophysiological data," *Integr. Comput.-Aided Eng.*, vol. 23, no. 1, pp. 81–97, Dec. 2015.

[13] R. Wang, J. Zhang, Y. Zhang, and X. Wang, "Assessment of human operator functional state using a novel differential evolution optimization based adaptive fuzzy model," *Biomed. Signal Process. Control*, vol. 7, no. 5, pp. 490–498, Sep. 2012.

[14] H.-R. Hou, Q.-H. Meng, M. Zeng, and B. Sun, "Improving classification of slow cortical potential signals for BCI systems with polynomial fitting and voting support vector machine," *IEEE Signal Process. Lett.*, vol. 25, no. 2, pp. 283–287, Feb. 2018.

[15] E. W. Sellers and E. Donchin, "A P300-based brain–computer interface: Initial tests by ALS patients," *Clin. Neurophysiol.*, vol. 117, no. 3, pp. 538–548, Mar. 2006.

[16] T. M. Vaughan *et al.*, "The wadsworth BCI research and development program: At home with BCI," *IEEE Trans. Neural Syst. Rehabil. Eng.*, vol. 14, no. 2, pp. 229–233, Jun. 2006.

[17] F.-B. Vialatte, M. Maurice, J. Dauwels, and A. Cichocki, "Steady-state visually evoked potentials: Focus on essential paradigms and future perspectives," *Prog. Neurobiol.*, vol. 90, no. 4, pp. 418–438, Apr. 2010.

[18] R. Ortner, B. Z. Allison, G. Korisek, H. Gaggl, and G. Pfurtscheller, "An SSVEP BCI to control a hand orthosis for persons with tetraplegia," *IEEE Trans. Neural Syst. Rehabil. Eng.*, vol. 19, no. 1, pp. 1–5, Feb. 2011.

[19] G. Hajcak, A. MacNamara, and D. M. Olvet, "Event-related potentials, emotion, and emotion regulation: An integrative review," *Develop. Neuropsychol.*, vol. 35, no. 2, pp. 129–155, Feb. 2010.

[20] G. Prasad, P. Herman, D. Coyle, S. McDonough, and J. Crosbie, "Applying a brain-computer interface to support motor imagery practice in people with stroke for upper limb recovery: A feasibility study," *J. NeuroEng. Rehabil.*, vol. 7, no. 1, Dec. 2010.

[21] K.-J. Chiang, C.-S. Wei, M. Nakanishi, and T.-P. Jung, "Boosting template-based SSVEP decoding by cross-domain transfer learning," *J. Neural Eng.*, vol. 18, no. 1, Feb. 2021, Art. no. 016002.

[22] M. Xu *et al.*, "Implementing over 100 command codes for a high-speed hybrid brain-computer interface using concurrent P300 and SSVEP features," *IEEE Trans. Bio. Eng.*, vol. 67, no. 11, pp. 1746–1752, Nov. 2020.

[23] W. M. Perlstein, M. A. Cole, M. Larson, K. Kelly, P. Seignourel, and A. Keil, "Steady-state visual evoked potentials reveal frontally-mediated working memory activity in humans," *Neurosci. Lett.*, vol. 342, no. 3, pp. 191–195, May 2003.

[24] C. Jia, X. Gao, B. Hong, and S. Gao, "Frequency and phase mixed coding in SSVEP-based brain-computer interface," *IEEE Trans. Biomed. Eng.*, vol. 58, no. 1, pp. 200–206, Jan. 2011.

[25] Z. Lin, C. Zhang, W. Wu, and X. Gao, "Frequency recognition based on canonical correlation analysis for SSVEP-based BCIs," *IEEE Trans. Biomed. Eng.*, vol. 53, no. 12, pp. 2610–2614, Dec. 2006.

[26] M. Cheng, X. Gao, S. Gao, and D. Xu, "Design and implementation of a brain-computer interface with high transfer rates," *IEEE Trans. Biomed. Eng.*, vol. 49, no. 10, pp. 1181–1186, Oct. 2002.

[27] Y. Zhang *et al.*, "Multiway canonical correlation analysis for frequency components recognition in SSVEP-based BCIs," in *Proc. ICONIP*, Shanghai, China, 2011, pp. 287–295.

[28] J. Pan, X. Gao, F. Duan, Z. Yan, and S. Gao, "Enhancing the classification accuracy of steady-state visual evoked potential-based brain–computer interfaces using phase constrained canonical correlation analysis," *J. Neural Eng.*, vol. 8, no. 3, May 2011, Art. no. 036027.

[29] Y. Zhang, G. Zhou, J. Jin, M. Wang, X. Wang, and A. Cichocki, "L1-regularized multiway canonical correlation analysis for SSVEP-based BCI," *IEEE Trans. Neural Syst. Rehabil. Eng.*, vol. 21, no. 6, pp. 887–896, Nov. 2013.

[30] Y. Zhang, G. Zhou, J. Jin, X. Wang, and A. Cichocki, "Frequency recognition in SSVEP-based BCI using multiset canonical correlation analysis," *Int. J. Neural Syst.*, vol. 24, no. 4, Jun. 2014, Art. no. 1450013.

[31] Z. Li, K. Liu, X. Deng, and G. Wang, "Spatial fusion of maximum signal fraction analysis for frequency recognition in SSVEP-based BCI," *Biomed. Signal Process. Control*, vol. 61, Aug. 2020, Art. no. 102042.

[32] H. Wang, Y. Sun, Y. Li, S. Chen, and W. Zhou, "Inter- and intra-subject template-based multivariate synchronization index using an adaptive threshold for SSVEP-based BCIs," *Frontiers Neurosci.*, vol. 14, p. 717, Sep. 2020.

[33] H. Wang *et al.*, "Discriminative feature extraction via multivariate linear regression for SSVEP-based BCI," *IEEE Trans. Neural Syst. Rehabil. Eng.*, vol. 24, no. 5, pp. 532–541, May 2016.

[34] Y. Zhang, P. Xu, K. Cheng, and D. Yao, "Multivariate synchronization index for frequency recognition of SSVEP-based brain–computer interface," *J. Neurosci. Methods*, vol. 221, pp. 32–40, Jan. 2014.

[35] Y. Zhang, D. Guo, P. Xu, Y. Zhang, and D. Yao, "Robust frequency recognition for SSVEP-based BCI with temporally local multivariate synchronization index," *Cognit. Neurodyn.*, vol. 10, no. 6, pp. 505–511, Jul. 2016.

[36] H. Wang and D. Xu, "Comprehensive common spatial patterns with temporal structure information of EEG data: Minimizing nontask related EEG component," *IEEE Trans. Biomed. Eng.*, vol. 59, no. 9, pp. 2496–2505, Sep. 2012.

[37] H. Wang, "Temporally local maximum signal fraction analysis for artifact removal from biomedical signals," *IEEE Trans. Signal Process.*, vol. 58, no. 9, pp. 4919–4925, Sep. 2010.

[38] Y. Zhang, D. Guo, D. Yao, and P. Xu, "The extension of multivariate synchronization index method for SSVEP-based BCI," *Neurocomputing*, vol. 269, pp. 226–231, Dec. 2017.

[39] S. Lemm, B. Blankertz, G. Curio, and K.-R. Muller, "Spatio-spectral filters for improving the classification of single trial EEG," *IEEE Trans. Biomed. Eng.*, vol. 52, no. 9, pp. 1541–1548, Sep. 2005.

[40] F. Qi, Y. Li, and W. Wu, "RSTFC: A novel algorithm for spatio-temporal filtering and classification of single-trial EEG," *IEEE Trans. Neural Netw. Learn. Syst.*, vol. 26, no. 12, pp. 3070–3082, Dec. 2015.

[41] K. K. Ang, Z. Y. Chin, C. Wang, C. Guan, and H. Zhang, "Filter bank common spatial pattern algorithm on BCI competition IV datasets 2a and 2b," *Frontiers Neurosci.*, vol. 6, p. 39, Mar. 2012.

[42] X. Chen *et al.*, "Filter bank canonical correlation analysis for implementing a high-speed SSVEP-based brain-computer interface," *J. Neural Eng.*, vol. 12, no. 4, pp. 1541–1548, Jun. 2015.

[43] M. Vetterli and C. Herley, "Wavelets and filter banks: Theory and design," *IEEE Trans. Signal Process.*, vol. 40, no. 9, pp. 2207–2232, Sep. 1992.

[44] F. Di Russo and D. Spinelli, "Electrophysiological evidence for an early attentional mechanism in visual processing in humans," *Vis. Res.*, vol. 39, no. 18, pp. 2975–2985, Sep. 1999.

[45] Y. Wang, X. Chen, X. Gao, and S. Gao, "A benchmark dataset for SSVEP-based Brain–Computer interfaces," *IEEE Trans. Neural Syst. Rehabil. Eng.*, vol. 25, no. 10, pp. 1746–1752, Oct. 2017.